Structural characterizations of histidine-containing tripeptides complexed with zinc and cadmium dications using IRMPD spectroscopy and theoretical calculations

Samantha K. Walker, ¹ Brandon C. Stevenson, ¹ Fan Yang, ¹ Roland M. Jones III, ¹ Giel Berden, ² Jonathan Martens, ² Jos Oomens, ^{2,3} and P. B. Armentrout ¹

¹Department of Chemistry, University of Utah, 315 S. 1400 E. Rm. 2020, Salt Lake City, Utah 84112, USA

²Radboud University, Institute for Molecules and Materials, FELIX Laboratory, Toernooiveld 7, 6525 ED Nijmegen, The Netherlands

³van't Hoff Institute for Molecular Sciences, University of Amsterdam, Science Park 904, NL-1098 XH Amsterdam, The Netherlands

M²⁺(HisAlaAla), M²⁺(AlaHisAla), **Abstract:** Metalated gas-phase complexes, M²⁺(AlaAlaHis), where M = Zn and Cd, were examined using infrared multiple photon dissociation (IRMPD) spectroscopy with light from a free-electron laser (FEL). These complexes were chosen because they provide model systems for metal binding to proteins. Complementary simulated annealing calculations were performed to determine energetically low-lying conformers and isomers of these structures. Quantum chemical calculations were used to optimize the structures at the B3LYP level of theory using 6-311+G(d,p) and def2-TZVP basis sets for zinc and cadmium complexes, respectively. IRMPD and calculated linear absorption spectra were compared to evaluate which structures are present. Relative energies of the various species were evaluated using single-point energy calculations for low-lying structures at the B3LYP, B3P86, and MP2(full) levels using 6-311+G(2d,2p) and def2-TZVPP basis sets. For species with histidine at a terminal position (AAH or HAA), the conformations that best reproduce the IRMPD spectra are charge-solvated (CS) conformers, where the metal dication binds to the amine and carbonyl groups of the peptide backbone and to the nitrogen of the histidine side chain, along with contributions from an iminol structure for AAH. The species with the histidine in the center position (AHA) adopt an iminol structure, where the metal dication binds to the backbone iminol nitrogens, the α -amine, π -imine, and the carbonyl of the C-terminus.

Introduction

Zinc is the second most abundant trace metal found in eukaryotic organisms and therefore has many influential biological functions.[1, 2] Zinc finger proteins are numerous transcription factors in the human genome and are partially characterized by their binding motifs. Eight such binding motifs have been characterized according to their main-chain conformation and secondary structure, one of which binds zinc to two cysteine and two histidine residues.[3, 4] The binding motifs and various domains allow zinc finger proteins to play many different roles in gene regulation under various cellular environments and other stimuli.[5] Here, we use small-scale systems with biomimetic features of zinc finger systems in order to better understand the peptide conformations that bind zinc.

Combining the active chelation site of the imidazole side chain of the histidine (His) residue with the less active side chain of alanine (Ala) provides a means to study how small histidine-containing peptides bind to metals. [6] Alanine was also chosen to facilitate comparison with previous work done by Dunbar, including dialanine, trialanine, and the analogous tripeptides of this study, HisAlaAla, AlaHisAla, and AlaAlaHis.[7, 8] Studies of these three tripeptides with a dication metal center (M²⁺) probe how the position of the histidine residue influences the binding site for the metal and the peptide conformation. Dunbar et al. examined these complexes for M = Ni and Cu using infrared multiple photon dissociation (IRMPD) spectroscopy in the gas phase.[8] This study helped our understanding of the various chelation patterns and binding configurations. Notably, Dunbar et al. found that the histidine side chain was not involved in the binding, but instead found an iminol binding motif (first identified previously in Ref [9]), in which the hydrogen on a backbone amide nitrogen migrates to the amide oxygen, providing a strong binding site for the metal cation.[8] In the condensed phase, imine binding to metal ions is facilitated by a proton transfer to the surrounding solvent. Utilizing gas-phase methods, metal chelated peptides can be studied structurally in the absence of solvent effects. The distinction between the gas and condensed phase presents opportunities for studies of solvation effects and facilitates understanding of complex systems that become more elusive with solvation and proton transfers.

In the present work, we extend this previous study by including the same three tripeptides but expanding the metals to include zinc and cadmium. Like nickel and copper, zinc and cadmium are transition metals, but have different valence electronic configurations that may influence their proclivity to form the iminol binding motif. Zinc and cadmium are both group-12 metals with the same valence electron configurations and 2+ oxidation states. Both metals are biologically relevant, although cadmium is an environmental pollutant and has been observed to replace zinc in various zinc finger motifs.[10, 11] The present study uses IRMPD to collect IR spectra of M^{2+} (HisAlaAla), M^{2+} (AlaHisAla), and M^{2+} (AlaAlaHis), where M = Zn and Cd. These experimental spectra are compared to calculated spectra of various low-energy conformers and isomers. This work is also an extension of many previous studies that have examined the structures of zinc and cadmium dications coordinating with amino acids and peptides in the gas-phase. These studies include the histidine (His) monomer, dimer, and dipeptide,[12-15] cysteine (Cys),[16] cysteine methyl ester (Cys-OMe),[16] methionine (Met),[17] glycine (Gly),[18] serine (Ser),[19] threonine (Thr),[18] aspartic acid (Asp),[20] glutamic acid (Glu),[21] asparagine (Asn),[22] glutamine (Gln),[23] lysine (Lys),[24] arginine (Arg),[25] phenylalanine (Phe),[26] tyrosine (Tyr),[26] and tryptophan (Trp).[26, 27]

Experimental and Computational Section

Mass Spectrometry and Photodissociation. Experiments were performed at the Free Electron Lasers for Infrared eXperiments (FELIX) Laboratory at Radboud University, the Netherlands.[28] The IRMPD spectroscopy experiments were conducted as described previously.[13] Briefly, spectroscopy was conducted using a quadrupole ion trap mass spectrometer (QIT-MS) modified to allow optical access to the ion cloud by the FEL beam.[29] The M²⁺(HisAlaAla), M²⁺(AlaHisAla), and M²⁺(AlaAlaHis) complexes, where M = Zn and Cd, were generated using an electrospray ionization (ESI) source from solutions containing 10 μM metal chloride salt and an equivalent amount of tripeptide in methanol. Reagents were obtained from commercial sources and used without further purification. Because the different complexes

of a given metal are isobaric, the instrument was flushed using solvent and we verified that the background ion signal did not contain carryover between samples. Although most spectra discussed in this paper were collected using the QIT-MS, select data were also collected using a home-built Fourier transform ion cyclotron resonance (FTICR) MS.[30, 31] With one exception, discussed below, the FTICR spectra match the QIT spectra and are therefore only shown in the Supplementary Information. Ions in either trap were irradiated with light from the FELIX laser over the approximate spectral range of $580 - 1900 \text{ cm}^{-1}$, although only a few vibrational bands are observed below 1000 cm^{-1} . Full spectra of the examined systems are presented in Figures S1 – S6. The bandwidth of the laser was 0.5% of the central frequency. The laser was operated at a 10 Hz macropulse repetition rate with energies up to 114 mJ per pulse. Laser attenuations were varied to ensure saturation did not obscure spectral features while still allowing weaker features to be observed. Fragments monitored are listed in the Supplementary Information Table S1.

IRMPD spectra were produced by plotting $Y = -\ln[\sum I_P/(\sum I_F + \sum I_P)]$, where I_P and I_F are the integrated intensities of the precursor and fragment ion mass peaks, as a function of the FEL laser frequency.[32] A linear correction was applied to the yield to account for frequency-dependent variation in the IR laser pulse energy. These corrections are appropriate for this experiment because the power dependence of the dissociation is practically linear until saturation occurs because of the incoherent nature of the multiple photon process, a phenomenon well detailed in the literature.[33]

Computational Details. A simulated annealing procedure detailed in previous publications was used to determine low-energy conformers.[34-38] Each unique conformer of the zinc-containing systems was then geometry optimized using the Gaussian16 suite of programs[39] at the B3LYP/6-31G(d) level of theory[40, 41] and then were further optimized using the B3LYP/6-311+G(d,p) level of theory. These structures were then used to generate cadmium-containing structures by replacing the zinc with cadmium and optimizing using the B3LYP/def2-TZVP level where the basis set on Cd has a small core (28 electron) effective core potential (ECP).[42, 43] Both the def2-TZVP basis set and the ECP were obtained from the Basis Set

Exchange.[44] Although many structures were calculated and are included in the Supplementary Information Table S2, only the lowest energy structures for each unique binding configuration are included in the main text of this paper.

Vibrational frequencies were calculated from the optimized structures and scaled by 0.975 to compare to the IRMPD spectra. To compensate for the finite laser bandwidth and unresolved rotational structure, a Gaussian line shape (25 cm⁻¹ FWHM) was used to broaden the calculated frequencies.[45] In previous studies, this scaling factor and line shape were demonstrated to provide an accurate description of the structural information for systems of similar size and make up.[8, 12-26] When comparing theoretical calculated spectra to experimental spectra, it is important to note that the intensities may differ since the calculated spectra correspond to a one-photon process whereas the IRMPD spectra require the absorption of multiple IR photons of resonant wavelength to induce dissociation.

Single-point energy (SPE) calculations of the optimized structures were performed at the B3LYP, B3P86, and MP2(full) levels of theory using the 6-311+G(2d,2p) and def-TZVPP basis sets for the zinc- and cadmium-containing species, respectively.[44] Zero-point energy (ZPE) corrections were applied to SPEs to provide 0 K relative enthalpies. Thermal corrections were calculated to obtain 298 K Gibbs energies using the rigid rotor/harmonic oscillator approximation with the calculated rotational constants and vibrational frequencies. When used for ZPE and thermal corrections, vibrational frequencies were scaled by 0.9896.[46] To determine whether the inclusion of dispersion forces affected the calculated geometries and energies, the B3LYP-GD3BJ level of theory was also used to optimize the ion geometry using the same basis sets.[47, 48] These structures were then used to calculate B3LYP-GD3BJ SPEs using the larger basis sets detailed above and are included for comparison below.

Results and Discussion

Nomenclature. Previous work has detailed the nomenclature used to identify the metalated peptide structures.[13] Briefly, the metal-binding sites ($N_{\alpha} = N$ -terminal amino nitrogen, $N_{\pi} =$

imidazole "pros" nitrogen, NH = amide backbone nitrogen, N = iminol backbone nitrogen where the hydrogen has migrated away, CO = carbonyl oxygen) are ordered moving along the peptide from the N-terminus to C-terminus and are listed in square brackets. Superscript numbers for N and CO specify the residue starting at the N-terminus. The designation of the metal binding site is then followed by the amino acid orientation, which is represented by characterization of dihedral angles along the peptide backbone as cis (c, for angles between 0° – 45°), gauche (g, 45° – 135°), or trans (t, 135° – 180°). Dihedrals are measured from the nitrogen atom of the N-terminus to the C-terminus ending with the carboxylic acid hydrogen. For iminol structures where a proton has migrated to a backbone carbonyl oxygen, CCOH dihedrals are added as subscripts to distinguish structures that otherwise would have the same metal-binding site and backbone orientation.

Relative Energies and Structures of $M^{2+}(AAH)$. As shown in Table 1 for $Zn^{2+}(AAH)$, there are three unique metal binding structures. At 298 K, all four levels of theory predict the same global minimum structure (GM), the pentadentate $[N_{\alpha}, N^2, N^3, CO^3, N_{\pi}]$ -ct_ctct_cttt, displayed in Figure 1. In this structure, the hydrogens originally on the backbone amide nitrogens N^2H and N^3H have migrated to CO^1H and CO^2H , yielding iminols where the N^2 and N^3 nitrogens are strong metal binding sites. Here, the CCOH dihedrals are both cis (indicated by the subscripts), with trans dihedrals leading to alternative structures that lie higher in energy by ~ 16 kJ/mol. B3LYP theory finds an alternative GM structure at 0 K, Table 1, a charge-solvated (CS) tetradentate structure, $[N_{\alpha}, CO^1, CO^2, N_{\pi}]$ -gtcttttt, which shows metal coordination with the amine nitrogen, the first two backbone carbonyl oxygens, and the π -imine nitrogen of the histidine side chain, Figure 1. The $[N_{\alpha}, CO^1, CO^3, N_{\pi}]$ -ttggtctt structure distorts the backbone such that the C^3 -terminal carbonyl binds to the metal rather than the C^2 carbonyl. This modification creates a more compact structure and increases the energy by 8-24 kJ/mol at 298 K from the lowest energy structure. No zwitterionic structures were observed among the low-energy structures for the $Zn^{2+}(AAH)$ system.

Table 2 shows that the lowest energy structure at all DFT levels of theory of the $Cd^{2+}(AAH)$ complex is the tetradentate $[N_{\alpha}, CO^{1}, CO^{2}, N_{\pi}]$ -gtcttttt in which the metal dication center binds with the α nitrogen, the backbone carbonyl groups on residues one and two, and the histidine side-

chain π nitrogen. Structurally, this conformer is the same as the Zn analog shown in Figure 1. Note that the analogous structure for Zn was 1 – 7 kJ/mol higher than the GM at the DFT levels but 20 kJ/mol for MP2 at 298 K. Instead, the Zn²+(AAH) [Na, N², N³, CO³, Nπ]-ctcttctt pentadentate iminol structure was the 298 K GM for all levels of theory. For Cd, this analogous structure remains the GM for MP2 at 298 K but lies 8 – 13 kJ/mol above the GM at the DFT levels. Overall, the relative stability of the CS structure compared to the pentadentate IM structure has been lowered by 14 – 17 kJ/mol at all levels of theory. We attribute this result to the higher charge density Zn ion binding more favorably with the negatively charged iminol positions, compared to the charge solvated (CS) structure found for the DFT GM of the cadmium complex. The next highest energy structure is [Na, CO¹, CO³, Nπ]-gtggtgtt, which is similar to the GM but replaces CO² coordination with CO³. The distortions needed for this change increase the energy by 14-24 kJ/mol. This structure is nearly identical to the zinc analogue, [Na, CO¹, CO³, Nπ]-ttggtctt. The differences in the backbone dihedrals are quite small, Zn²+-t140tggtc43tt versus Zd²+-g126tggtg50tt (where subscript numbers indicate the calculated backbone dihedral angles). No zwitterionic structures were found to be low in energy for this system.

Relative Energies and Structures of $M^{2+}(AHA)$. Table 3 shows that the lowest energy structure for $Zn^{2+}(AHA)$ at B3LYP and B3P86 levels of theory and 298 K is $[N_{\alpha}, N^2, N^3, CO^3]$ -ct_ctctttt, Figure 2. Here, the metal dication binds to two iminol nitrogens along with the amine nitrogen and the carbonyl of the C-terminus. In this case, the CO^2H hydrogen-bonds with the histidine side-chain N_{π} nitrogen, which leads to further migration of the hydrogen to N_{π} and a $CO^2 \cdot HN_{\pi}$ hydrogen bond in the final structure. The alternative $[N_{\alpha}, N^2, N^3, CO^3]$ -cttcttt structure is very similar with the distinction that the structure rotates the $CO^2 \cdot HN_{\pi}$ hydrogen bond to be a $CO^1 \cdot HN_{\pi}$ hydrogen bond, which increases the energy by 1 - 5 kJ/mol at 298 K. Because the proton is bound to N_{π} , both of these $[N_{\alpha}, N^2, N^3, CO^3]$ -cttctttt species are zwitterionic. These two structures lie much higher in relative energy for B3LYP-GD3BJ (by ~10 kJ/mol) and MP2 (25 – 30 kJ/mol) levels at 298 K. Instead, at these levels of theory, $[N_{\alpha}, N^2, N_{\pi}, N^3, CO^3]$ -ct_cgct_cttt is the GM (also at 0 K for B3P86). This pentadentate structure adds N_{π} to the metal coordination, thereby

removing the $CO \cdot HN_{\pi}$ hydrogen bonds. The $[CO^1, N_{\pi}, N^3H, CO^3]$ -ctcgtgtt structure is a CS structure that binds the metal to the backbone N^3H group, the N_{π} nitrogen, and two carbonyl oxygens. This structure lies 19-34 kJ/mol above the respective GMs. The $[N_{\alpha}, CO^1, CO^2, CO^3]$ -gtgttggt is a CS structure that creates a $N^3H \cdot N_{\pi}$ hydrogen bond. This structure lies 52-73 kJ/mol above the GM.

As for the Zn²⁺(AHA) analogue, Cd²⁺(AHA) has two unique iminol binding motifs with the metal center; however, four iminol structures are listed in Table 4 to account for the 298 K GM and the 0 K GM at the B3LYP-GD3BJ and MP2 levels of theory. The GM according to B3LYP and B3P86 is $[N_{\alpha}, N^2, N^3, CO^3]$ -ctctttt, as also found for the Zn analogue. If the hydrogen bond to the His side chain rotates from $CO^2 \bullet HN_{\pi}$ to $CO^1 \bullet HN_{\pi}$, one obtains $[N_{\alpha}, N^2, N^3, CO^3]$ -cttctcttt, which is nearly isoenergetic (within 1.2 kJ/mol at 298 K) at all levels of theory. Both $\lceil N_{\alpha},\,N^2,\,N^3,$ CO^3]-cttctttt structures involve a proton transfer from the amide nitrogen to N_{π} , such that these are zwitterionic species. The $[N_{\alpha}, N^2, N_{\pi}, N^3, CO^3]$ -ct_cgct_cttt structure is the calculated 298 K GM at the MP2 and dispersion-corrected DFT levels, similar to the Zn analogues. This structure lies ~5 kJ/mol above the GM at the B3LYP and B3P86 levels at 298 K (\sim 8 kJ/mol at 0 K). The $[N_{\alpha}, N^2,$ N_π, N³, CO³]-ct_ctct_tttt structure is the calculated 0 K GM for B3LYP-GD3BJ and MP2 levels of theory, Figure 2 and Table 4. This structure lies 2 – 12 kJ/mol above the respective 298 K GMs and 2 – 7 kJ/mol above the similar ct_ccgct_cttt conformer. Lying higher in energy (18 – 31 kJ/mol above the respective GMs), the $[CO^1, N_{\pi}, N^3H, CO^3]$ -ctcgtgtt structure is a CS structure that binds the metal to the backbone N^3H group and the N_{π} nitrogen, similar to the Zn analogue. The $[N_{\alpha}]$ CO^1 , CO^2 , CO^3]-gtgttggt structure is also a CS structure that has a $N^3H^{\bullet}N_{\pi}$ hydrogen bond. This structure lies 38 - 55 kJ/mol above the respective GMs.

Relative Energies and Structures of $M^{2+}(HAA)$. Table 5 shows that all levels of theory predict the lowest energy structure of $Zn^{2+}(HAA)$ is $[N_{\alpha}, N_{\pi}, N^2, N^3, CO^3]$ -ct_ctct_cttt, Figure 3. In this structure, the metal coordinates with the N-terminal amine nitrogen, the histidine side-chain π nitrogen, two backbone iminol nitrogens, and C-terminal carbonyl oxygen, in similar fashion to the $Zn^{2+}(AAH)$ GM. The $[N_{\alpha}, N_{\pi}, CO^1, CO^3]$ -gtcttgtt structure is a CS structure that replaces the

iminol coordination with the CO^1 group. This structure is 1-13 kJ/mol higher than the GM. The $[N_{\alpha}, N_{\pi}, CO^1, CO^3]$ -gtggtggc structure has the same metal coordination but lies 22-27 kJ/mol higher in energy than the $[N_{\alpha}, N_{\pi}, CO^1, CO^3]$ -gtcttgtt structure. Here, the C-terminus CO^3 •HO hydrogen bond has been broken and replaced with a CO^2 •HO hydrogen bond. The $[N_{\alpha}, N_{\pi}, CO^1, CO^2, CO^3]$ -ttcttgtt (22-33 kJ/mol higher than the GM) is similar to the second lowest state but becomes pentacoordinate by moving the CO^2 carbonyl within bonding distance of the zinc dication at the cost of relatively long Zn bonds to N_{α} , CO^1 , and CO^2 . No zwitterionic structures were observed among the low-energy structures for this system.

All four levels of theory (Table 6) agree that the GM of $Cd^{2+}(HAA)$ is $[N_{\alpha}, N_{\pi}, CO^{1}, CO^{2},$ CO^3]-gtcttggt, Figure 3. Here, the metal dication binds to the α nitrogen, histidine side-chain π nitrogen, and the backbone carbonyl groups of all three residues. The zinc analogue (Figure 3) is quite similar with Zn-t₁₆₀tcttgt₁₄₅t versus Cd-g₈₅tcttgg₁₃₁t. The backbone dihedral differences are clearly most distinct in the first dihedral. This difference changes the configuration of the CO¹ and CO² with respect to the metal. We ensured that substitution of the other metal in both structures collapsed to the structures already represented here. The $[N_{\alpha},\,N_{\pi},\,N^2,\,N^3,\,CO^3]$ -ctctcttt structure is an iminol structure that binds the two backbone nitrogens, the α nitrogen, histidine side-chain π nitrogen, and the terminal CO³ carbonyl to the metal dication center. Whereas this iminol structure was the GM in for $Zn^{2+}(HAA)$, here, it lies 4 - 14 kJ/mol above the GM at 298 K. This change is likely a result of the smaller, higher charge density zinc binding more favorably with the iminol site. In the $[N_{\alpha}, N_{\pi}, CO^1, CO^3]$ -gtggtggc structure, the backbone CO^2 interaction with the metal dication in the GM has been replaced with a CO²•HO hydrogen bond, costing 24 – 28 kJ/mol. The $Zn^{2+}(HAA)$ complex also has a lower energy $[N_{\alpha}, N_{\pi}, CO^{1}, CO^{3}]$ -gtcttgtt structure, but when the cadmium analogue of this structure is geometry optimized, it converges to the GM noted above. In this case, the larger size of the cadmium allows all three carbonyl groups to interact favorably with the metal center. Like for the M²⁺(AAH) complexes, the energy difference between the CS and the iminol structures for the zinc complex is much smaller than that of the cadmium analogues. No zwitterionic structures were among the lowest energy structures of this system.

Comparison of Experimental and Theoretical Spectra: M²⁺(AAH). Figure 4 shows the IRMPD action spectra of Zn²⁺(AAH) and comparisons to calculated spectra. The major features in the FTICR spectrum are centered at 1705, 1448, 1300, 1214, 1155, and 1085 cm⁻¹. The QIT spectrum adds bands at 1786, 1576, and 1522 cm⁻¹ and the band at 1300 broadens. The predicted GM $[N_{\alpha}, N^2, N^3, CO^3, N_{\pi}]$ -ct_ctct_cttt reproduces the FTICR spectrum well. Here, bands are predicted at 1721 and 1705 cm⁻¹ (CN² and CN³ stretch), 1680 cm⁻¹ (CO³ stretch and CO³H in-plane bend), 1497 cm⁻¹ (CN_π ring stretch), 1456 cm⁻¹ (C-terminus side-chain CH₂ bend), 1412 cm⁻¹ (mainly CO³H in-plane bend with nearby CCH bend), 1349 cm⁻¹ (histidine side-chain CH₂ wag), 1283 cm⁻¹ 1 (CO 1 H in-plane bend), 1169 cm $^{-1}$ (CO 3 H in-plane bend), 1128 cm $^{-1}$ (N $_{\alpha}$ H $_{2}$ wag), and 1075 cm $^{-1}$ ¹(N_αH₂ wag and N³C stretch). Notably, this spectrum does not reproduce the minor peak at 1786 cm⁻¹ and intensity in the 1500 – 1600 cm⁻¹ range observed in the QIT spectrum. These observations suggest the presence of $[N_{\alpha}, CO^1, CO^2, N_{\pi}]$ -gtctttt, whose spectrum reproduces this peak well with a CO³ stretch (1780 cm⁻¹) as well as intense peaks at 1598 cm⁻¹ (mainly N₀H₂ scissor with CO¹ and CO^2 stretches), 1578 cm⁻¹ (CC ring stretch with CN_{α} backbone stretches), 1575 cm⁻¹ (CO¹ stretch with CN³ stretch), 1534 cm⁻¹ (CN²H in-plane bend), 1456 cm⁻¹ (CN_α ring stretch with nearby CH₂ scissor), 1154 and 1153 cm⁻¹ (CO³H rock and $N_{\alpha}H_2$ wag), and 1049 cm⁻¹ ($N_{\alpha}H_2$ wag) . The higher energy $[N_{\alpha}, CO^{1}, CO^{3}, N_{\pi}]$ -ttggtctt structure has a predicted spectrum with its most intense band at 1640 cm⁻¹, which disagrees with the observed spectrum. We conclude that the GM structure is present exclusively in the FTICR, along with contributions from the low-lying $[N_{\alpha}]$ CO^1 , CO^2 , N_{π}]-gtcttttt species in the QIT. Here, we believe the differences are a result of the trapping gas needed in the QIT, which allows for rf heating to occur in the trap, potentially populating the low-lying species. Because no trapping gas is needed for the FTICR, we believe that this spectrum is a good representation of what thermalized species can be extracted from the electrospray source.[14]

Figure 5 shows the IRMPD action spectrum of Cd²⁺(AAH) taken in the QIT and comparison to calculated spectra and the Zn²⁺(AAH) QIT spectrum. FTICR measurements of this system show a similar spectrum but with more noise, as shown in the Supplementary Information

Figure S2. Although the relative intensities differ in the Cd²⁺(AAH) and Zn²⁺(AAH) experimental spectra, the main bands are similar, suggesting similar binding structures for the peptides with both metals. Indeed, for the Cd system, the major features center at 1794, 1715, 1672, 1611, 1578, 1526, 1447, 1388, 1334, 1221, 1153, and 1086 cm⁻¹. The spectrum of the predicted GM, $[N_{\alpha}, CO^{1}, CO^{2},$ N_{π}]-gtcttttt reproduces much of the experimental spectrum quite well, although it misses the features from the experimental spectrum at 1715 and 1672 cm⁻¹. Specifically, the calculated spectrum for $[N_{\alpha}, CO^1, CO^2, N_{\pi}]$ -gtcttttt has peaks at 1779 cm⁻¹ (CO³ stretch), 1611 cm⁻¹ (CO¹ and CO² stretches and N_αH₂ scissor), 1600 cm⁻¹ (N_αH₂ scissor), 1579 cm⁻¹ (CO¹, CO², and CC ring stretches), 1577 cm⁻¹ (CO¹, CO², CC ring stretches), 1525 cm⁻¹ (CN²H and CN³H bends), 1393 cm⁻¹ (alanine side-chain CH₃ umbrella), 1375 and 1337 cm⁻¹ (CO³H in-plane bend), 1271 cm⁻¹ (histidine side-chain ring stretches), 1149 cm⁻¹ (CO³H in-plane bend and N_αH₂ wag), and 1065 cm⁻¹ ¹ (N_αH₂ twist). As for the Zn analogue, the bands near 1700 cm⁻¹ are reproduced by the iminol structure, [N₀, N², N³, CO³, N_{\pi}]-ct_ctct_cttt, which has bands at 1721 cm⁻¹ (CN² stretch, CN³ stretch, CO¹H and CO²H in-plane bends), 1708 cm⁻¹ (CN² stretch, CN³ stretch, CO¹H and CO²H in-plane bends), and 1685 cm⁻¹ (CO³ stretch). It also has intensity at 1294 cm⁻¹ (CO²H in-plane bend) and 1278 cm⁻¹ (CO¹H in-plane bend) and reproduces the bands at 1153 and 1086 cm⁻¹, with predicted peaks at 1163 cm⁻¹ (CO³H in-plane bend) and 1073 cm⁻¹ (N_{α}H₂ wag). The [N_{α}, CO¹, CO³, N_{π}]gtggtgtt calculated spectrum does not reproduce the experimental spectrum well, with intense features at 1654 and 1470 cm⁻¹ that are not observed experimentally. We conclude that the GM and the iminol structure are both present, where the presence of the latter is consistent with the relatively low calculated energy at the MP2 level of theory (1.2 kJ/mol at 298 K). Note that the relative populations here are inverted from those of the Zn analogue. This population inversion is consistent with the relative magnitudes of the peaks in the Zn²⁺(AAH) versus Cd²⁺(AAH) spectra, Figure 5.

Comparison of Experimental and Theoretical Spectra: M²⁺(AHA). Photodissociation of Zn²⁺(AHA) was monitored from 580 to 1900 cm⁻¹. FTICR experiments show the same spectrum but with lower signal and more noise than the QIT experiments, Figure S3. Figure 6 shows the

IRMPD action spectrum of Zn²⁺(AHA) starting at 1000 cm⁻¹ and comparison of five calculated spectra. The major features observed are centered at 1722, 1662, 1451, 1286, 1171, and 1089 cm⁻¹ ¹. The B3LYP-GD3BJ and MP2 GM, $[N_{\alpha}, N^2, N_{\pi}, N^3, CO^3]$ -ct_cgct_cttt, has a predicted spectrum that reproduces the major spectral features of the experimental spectrum. Specifically, bands are predicted at 1742 cm⁻¹ (CN² stretch), 1714 cm⁻¹ (CN³ stretch), 1643 cm⁻¹ (CO³ stretch), 1464 and 1463 cm⁻¹ (C-terminus CH₂ scissor), 1459 and 1458 cm⁻¹ (N-terminus CH₂ scissor), 1377 cm⁻¹ (Nterminus CH₃ umbrella), 1352 cm⁻¹ (histidine side-chain CH₂ wag), 1301 cm⁻¹ (ring stretch and HCC in-plane bend), 1294 cm⁻¹ (CO³H in-plane bend), 1283 cm⁻¹ (CO¹H and CO²H in-plane bends), 1278 cm⁻¹ (CO¹H and CO²H in-plane bends and N_αH₂ twist), 1188 and 1181 cm⁻¹ (CO¹H and CO²H in-plane bends), 1176 cm⁻¹ (CO³H in-plane bend), 1102 cm⁻¹ (CN³ stretch and nearby CH₃ bend), 1084 cm⁻¹ (ring CN_{π} stretch), 1070 cm⁻¹ (CN_{α} stretch), 1056 cm⁻¹ (N_{α}H₂ wag and N²C stretch), and 1042 cm⁻¹ (N³C stretch). We conclude that the B3LYP-GD3BJ and MP2 GM structure is present, consistent with its low calculated energy. The other four calculated spectra shown all have intense bands that are not observed experimentally, suggesting that these species are not populated significantly if at all. In particular for the B3LYP and B3P86 GM, [Nα, N², N³, CO³]ct_ctctttt, intense bands at 1612 and 1611 cm⁻¹ (CO³ stretch and N₀H₂ scissor) and 1598 cm⁻¹ (CO² stretch and CC ring stretch) lie in a region where little intensity is seen experimentally.

Photodissociation of Cd²⁺(AHA) was monitored from 580 to 1900 cm⁻¹. Figure 7 shows the IRMPD action spectrum of Cd²⁺(AHA) starting at 1000 cm⁻¹ and comparison to five calculated spectra and that of Zn²⁺(AHA). FTICR experiments show the same spectrum but with less signal and more noise than the QIT experiments, Figure S4. The major features are similar to those observed in the zinc system, especially if the broad band at 1716 cm⁻¹ is saturated. Other bands observed are centered at 1589, 1449, 1288 (broad), 1209, 1158, and 1089 cm⁻¹. As for the Zn analogue, the 298 K B3LYP-GD3BJ and MP2 GM, [Nα, N², Nπ, N³, CO³]-ctctctcttt, has a spectrum that reproduces the experimental spectrum quite well with features at 1731 cm⁻¹ (CN² stretch), 1714 cm⁻¹ (CN³ stretch), 1647cm⁻¹ (CO³ stretch), 1614 cm⁻¹ (NαH₂ scissor), 1497 cm⁻¹ (ring CNπ stretch), 1463 and 1462 cm⁻¹ (alanine side-chain CH₂ scissor), 1455 cm⁻¹ (N-terminus CH₂ scissor),

1447 cm⁻¹ (ring CN_πH bend), 1440 cm⁻¹ (histidine side-chain CH₂ scissor), 1309 cm⁻¹ (CO¹H inplane bend and N_αH₂ twist), 1305 cm⁻¹ (histidine side-chain ring stretches), 1300 cm⁻¹ (CO³H inplane bend and nearby NCH in-plane bend), 1280 and 1275 cm⁻¹ (CO¹H and CO²H in-plane bends), 1230 cm⁻¹ (CO¹H, CO²H in-plane bends and N_αH₂ twist), 1172 cm⁻¹ (CO³H in-plane bend), 1107 cm⁻¹ (N³C stretch and CH₃ twist), and 1045 cm⁻¹ (N_{α}H₂ wag). The analogous [N_{α}, N², N_{π}, N³, CO³]-ct_ctct_tttt structure, the 0 K B3LYP-GD3BJ and MP2 GM, has a fairly similar spectrum. The one observed band that is not reproduced particularly well by either of these predicted spectra is a weak band at 1589 cm⁻¹. For metalated amino acids, [12, 13, 16, 17, 19, 21, 23, 33, 49-52] the $N_{\alpha}H_2$ scissors motion (predicted here at 1614 cm⁻¹) can be red-shifted due to anharmonicity, such that this may reproduce this experimental feature. This band is also potentially associated with the B3LYP and B3P86 GM, [N_α, N², N³, CO³]-ct_ctctttt, which has an intense feature at 1583 cm⁻¹ (CO¹ stretch), along with peaks at 1693 cm⁻¹ (CN³ stretch), 1636 cm⁻¹ (CO³ stretch), 1435 cm⁻¹ (CN_{π}H bend), and 1176 cm⁻¹ (CO³H in-plane bend). The latter features all lie underneath bands associated with the B3LYP-GD3BJ and MP2 GM. Likewise, the spectrum for $[N_{\alpha}, N^2, N^3, CO^3]$ -cttctcttt is fairly similar to the spectrum of the related ctctcttt conformer and therefore could also be populated. The other structure shown, [CO¹, N_{π} , N³H, CO³]-ctcgtgtt, has a spectrum with intense bands that that are not observed experimentally. We conclude the B3LYP-GD3BJ and MP2 298 K GM species is present, consistent with its low calculated energy, along with a possible minor contribution of the B3LYP and B3P86 GM structure. Low-energy variants of both structures may also be populated.

Comparison of Experimental and Theoretical Spectra: $M^{2+}(HAA)$. Photodissociation of $Zn^{2+}(HAA)$ was monitored from 580 to 1900 cm⁻¹, but only using the QIT. Figure 8 shows the IRMPD action spectrum of $Zn^{2+}(HAA)$ starting at 1000 cm⁻¹ and comparison to calculated spectra. The major features center at 1648, 1580 (broad), 1537 cm⁻¹, with small peaks at 1457, 1301, and 1175 cm⁻¹. Although not the lowest energy structure, $[N_{\alpha}, N_{\pi}, CO^{1}, CO^{2}, CO^{3}]$ -ttcttgtt reproduces the experimental spectrum reasonably well. There is agreement in position of all peaks with some discrepancies in the relative intensity, particularly between the 1580 and 1537 cm⁻¹ peaks. The

peaks in the calculated spectrum that correspond to the experimental peaks are 1660 cm⁻¹ (CO¹, CO², CO³ stretches and $N_{\alpha}H_2$ scissor), 1611 cm⁻¹ ($N_{\alpha}H_2$ scissor), 1572 cm⁻¹ (CO³ stretch and $N_{\alpha}H_2$ scissor), 1538 cm⁻¹ (CN³H in-plane bend), 1512 cm⁻¹ (CN²H in-plane bend), 1454 cm⁻¹ (histidine side-chain CH₂ scissor), 1331 cm⁻¹ (CO³H in-plane bend), and 1184 cm⁻¹ (CO³H in-plane bend). The [N_{α} , N_{π} , N^2 , N^3 , CO³]-ct_ctct_cttt structure is energetically the lowest at all levels of theory; however, its predicted spectrum does not reproduce the experimental spectrum well. Specifically, the calculated spectrum contains an intense peak at 1733 cm⁻¹ (CN² stretch) that is not found in the experimental spectrum. Likewise, the low-energy [N_{α} , N_{π} , CO¹, CO³]-gtcttgtt structure does not have a predicted spectrum that adequately corresponds to the experimental spectrum, including an intense feature at 1601 cm⁻¹ (CO¹ and CO³ stretch) that is not observed experimentally. We conclude that the [N_{α} , N_{π} , CO¹, CO², CO³]-ttcttgtt structure is present.

Photodissociation of Cd²⁺(HAA) was monitored from 580 to 1900 cm⁻¹ using the QIT. Figure 9 shows the IRMPD action spectrum of Cd²⁺(HAA) starting at 1000 cm⁻¹ and comparison to calculated spectra and that of Zn²⁺(HAA). The spectrum is similar to the Zn analogue with major features centered at 1653, 1582, and 1523 cm⁻¹, along with minor peaks at 1457, 1296, and 1178 cm⁻¹. As for the Zn analogue, the $[N_{\alpha}, N_{\pi}, CO^1, CO^2, CO^3]$ -gtcttggt structure, now the GM, has a spectrum that nicely reproduces the major features of the experimental spectrum. Specifically, it has bands at 1656 cm⁻¹ (mainly CO³ stretch and COH in-plane bend with CO¹ and CO² stretches), 1574 cm⁻¹ (mainly CO² stretch and CN³H in-plane bend), 1524 cm⁻¹ (CN²H in-plane bend), and 1522 cm⁻¹ (CN³H in-plane bend). The minor peaks observed can be related to predicted bands at 1462 cm⁻¹ (CH₂ scissor of alanine side-chains), 1285 cm⁻¹ (histidine side-chain ring stretches), and 1181 cm⁻¹ (CO³H in-plane bend). The calculated GM does include a band at 1614 cm⁻¹ (mainly CO¹ stretch with nearby CCH and CN²H in-plane bends) that does not correspond well with the experimental spectrum. We think that this peak may correspond to the shoulder seen in the experimental spectrum at approximately 1590 cm⁻¹. Because CO¹ binds to the cadmium ion (the CO bond is actually nearly perpendicular to the O-Cd bond), this frequency may be sensitive to whether the calculation overestimates or underestimates the strength of this CO¹–Cd interaction.

Because of this discrepancy, we investigated whether other levels of theory might match the experiment better, therefore, additional calculations were done with levels of theory suggested recently by Rodrigues-Oliveira et al.,[53] but these did not improve the comparison and indeed are in worse agreement than the B3LYP calculated spectrum. These results can be seen in the Supplementary Information, Figure S7.

Similar to the Zn analogue, the $[N_{\alpha}, N_{\pi}, N^2, N^3, CO^3]$ -ctctctcttt and the $[N_{\alpha}, N_{\pi}, CO^1, CO^3]$ -gtggtggc do not have predicted spectra that correspond to the experimental spectrum well. We conclude that the DFT and MP2 GM structure is present, consistent with its low energy. The comparison of the spectra for $Zn^{2+}(HAA)$ and $Cd^{2+}(HAA)$ makes it clear that they have similar binding motifs, consistent with the assignment made above for $Zn^{2+}(HAA)$. We attribute the change in relative energy between zinc and cadmium to the lower charge density on the cadmium metal center, which permits a less sterically hindered structure and leads to changes in the dihedral angles (ttcttgtt versus gtcttggt, Figure 3).

Iminol Tautomeric Probability. In model systems of dialanine and trialanine, Dunbar et al. assessed the factors that influence whether an IM versus a CS binding configuration is adopted.[7] Dunbar pointed to factors that include the charge of the metal ion, electrostatics, and stronger ion binding, which all correlate to a preference for IM conformation. Dunbar noted that zinc and cadmium are both transition metals and doubly charged, therefore concluding that they should favor IM coordination. He also defined an electrostatic parameter as q/R, where q is the charge of the ion and R is the distance from the metal ion to the effective charge at the chelation site. Using this parameter, Dunbar concluded that again both zinc and cadmium should prefer IM coordination. Dunbar also explored other factors that could influence the binding configuration such as "hard" versus "soft" metals and the length of the peptide (i.e., dipeptide versus tripeptide). He concluded that this metal characteristic was not helpful and that the length of the peptide resulted in nearly identical results despite the different number of Lewis-basic chelation points available.

In the present work, we find the IM to be dominant for the AHA systems, present for the AAH systems, and not a main contributor for HAA systems, Table 7. Thus, the AHA systems correspond well with the assessments of Dunbar. The AAH systems demonstrate that the higher charge density of zinc leads it to favor the IM structure, whereas the IM structure is present for Cd²⁺(AAH) but not dominant. In contrast, the HAA systems are not consistent with Dunbar's general assessments. However, the calculated energies of the M²⁺(HAA) systems indicate that the higher charge density of Zn favor IM compared to Cd, which does correlate to what Dunbar predicted. Further, we note that the Zn²⁺(HAA) calculated GM is an IM structure but does not reproduce the experimental spectrum well. We attribute the HAA systems being CS to an inability to transfer the proton along the backbone that is needed to form an IM. This challenge has been observed and discussed in the gas-phase in much of Dunbar's previous work;[7, 54] however, a mechanism for this rearrangement has not been worked out in any detail (and is beyond the scope of the present contribution). We hypothesize that the proximity of the histidine side chain to the N-terminus imposes some restrictions on this transformation, which presumably occurs in solution.

Comparison to Ni and Cu analogues. When Dunbar et al. used IRMPD to study the analogous peptides with Ni and Cu, they calculated that iminol structures were the lowest energy species for all systems.[8] In contrast to the iminol structures observed for Zn and Cd, the nickel and copper structures adopted four-coordinate square-planar configurations. This is a result of the open-shell character of these two metal cations (triplet spin for Ni²⁺ and doublet spin for Cu²⁺), which leads to directionality in the bonding that contrasts with the spherical closed-shell electron configurations of Zn²⁺ and Cd²⁺. Four of the structures that Dunbar et al. investigated could be clearly identified as having square-planar iminol (IM) structures that were the calculated global minimum, whereas the other two showed formation of the charge-solvated (CS) structures that were not the calculated GM or a mixture of the iminol and charge solvated structures, Table 7.

Dunbar et al. attributed this observation to the instrument type along with conditions in the source and ion trap.

More specifically, the Ni²⁺(AAH) spectra suggested a mixed population of iminol and charge-solvated structures, $[N_{\alpha}, N^2, N^3, CO^3]$ and $[N_{\alpha}, CO^1, CO^2, CO^3, N_{\pi}]$, whereas $Cu^{2+}(AAH)$ was a reasonably pure population of the former iminol structure. Likewise, the $Zn^{2+}(AAH)$ and $Cd^{2+}(AAH)$ spectra here suggest a mixture of the $[N_{\alpha}, N^2, N^3, CO^3, N_{\pi}]$ -ctctctcttt iminol and the charge-solvated $[N_{\alpha}, CO^1, CO^2, N_{\pi}]$ -gtcttttt with the relative populations inverted between these two metals. Note that the iminol structure for these two metals has added metal coordination to the side chain compared to the Ni and Cu complex structures.

The Ni²⁺(AHA) and Cu²⁺(AHA) spectra suggest nearly pure populations of the iminol structure, $[N_{\alpha}, N^2, N^3, CO^3]$. Likewise, the Zn²⁺(AHA) and Cd²⁺(AHA) spectra are reproduced primarily by the spectra predicted for the MP2 GMs, $[N_{\alpha}, N^2, N_{\pi}, N^3, CO^3]$ -ct_cgct_cttt, where again coordination to N_{π} has been added compared with the open-shell metal dications. It is also possible that the Cd²⁺(AHA) spectrum has a contribution from the $[N_{\alpha}, N^2, N^3, CO^3]$ -ct_ctctttt iminol structure, comparable to the findings of Dunbar et al.

The Ni²⁺(HAA) spectrum suggests a reasonably pure population of the iminol structure, $[N_{\alpha}, N^2, N^3, CO^3]$, whereas the Cu²⁺ (HAA) spectrum suggests a charge-solvated structure, $[N_{\pi}, CO^1, CO^2, CO^3]$, with some iminol contribution. The Zn²⁺(HAA) and Cd²⁺(HAA) spectra are reasonably reproduced by spectra predicted for $[N_{\alpha}, N_{\pi}, CO^1, CO^2, CO^3]$ -xtcttgxt. These results mirror that for Cu²⁺ with addition of N_{α} coordination. Again, Zn^{2+} and Cd^{2+} prefer coordination to the His side chain, whereas Ni²⁺ does not.

Conclusions

IRMPD spectroscopy was used to measure the IR spectra of the metalated gas-phase structures of M^{2+} (HisAlaAla), M^{2+} (AlaHisAla), and M^{2+} (AlaAlaHis), where M = Zn and Cd. These peptides were chosen for this investigation to combine the active chelation site of the

histidine side chain with the less active alanine side-chain to systematically probe how biologically relevant metals might bind in metalloproteins. The resulting spectra were compared to calculated spectra at the B3LYP/6-311+G(d,p) and B3LYP/def2-TZVP levels of theory for Zn and Cd species, respectively. There is good agreement between the Zn²⁺(AAH) experimental spectrum and the calculated GM $[N_{\alpha}, N^2, N^3, CO^3, N_{\pi}]$ -ct_ctct_cttt spectrum for most features, but some population of $[N_{\alpha}, CO^1, CO^2, N_{\pi}]$ -gtcttttt (low in energy at the B3LYP, B3LYP-GD3BJ, and B3P86 levels) is needed to fully explain all spectral features. The same is true for the Cd²⁺(AAH) system, although the relative populations of the iminol (now low lying at the MP2 level) and chargesolvated (now the GM at all levels) structures have inverted. In $Zn^{2+}(AHA)$, the $[N_{\alpha}, N^2, N_{\pi}, N^3,$ CO³]-ct_cgct_cttt structure (the MP2 and B3LYP-GD3BJ GM) has a predicted spectrum that reproduces the experimental spectrum well. For the Cd²⁺(AHA), the analogous structure (again the MP2 and B3LYP-GD3BJ GM) also dominates, but a $[N_{\alpha}, N^2, N^3, CO^3]$ -ctctttt structure (the B3LYP and B3P86 GM) may also make a minor contribution. For Zn²⁺(HAA) and Cd²⁺(HAA), the $[N_{\alpha}, N_{\pi}, CO^{1}, CO^{2}, CO^{3}]$ -xtcttgxt structure reproduces the experimental spectrum very well. Although this species is the GM at all levels of theory for the Cd complex, it is not the lowest energy structure for the Zn complex at any level of theory, but is low lying at the B3LYP and B3LYP-GD3BJ levels. Overall, B3LYP-GD3BJ calculations are the most consistent in identifying the observed structure, although only MP2 theory correctly suggest that the iminol structure of Cd²⁺(AAH) is low-lying and therefore might be populated as observed. None of the levels of theory predicts the observed Zn²⁺(HAA) structure is low lying.

The experiments and calculations for the metalated species with histidine at a terminal position (AAH or HAA) show that charge-solvated (CS) conformers reproduce the IRMPD spectra most closely; the metal dication binds to the amine and carbonyl groups of the peptide backbone and the nitrogen of the histidine side chain, although the presence of an iminol structure for the AAH conformations is needed as well and dominates for Zn. The metalated species with the histidine in the center position (AHA) possess an iminol structure, where the metal dication binds to the backbone iminol nitrogens, the α -amine, π -imine, and the carbonyl of the C-terminus. For

nickel and copper complexes, Dunbar et al. found that two-thirds of the structures adopt the iminol binding motif, which are square-planar configurations for these metals, specifically $Cu^{2+}(AAH)$, $Cu^{2+}(AHA)$, $Ni^{2+}(AHA)$, and $Ni^{2+}(HAA)$. The other two complexes, $Cu^{2+}(HAA)$ and $Ni^{2+}(AAH)$, have charge-solvated structures with some contribution of iminol structures as well. Notably, the Zn^{2+} and Cd^{2+} analogues are generally penta-coordinate, often adding coordination to the N_{π} nitrogen of the His side chain compared to the four-coordinate square-planar geometries of the open-shell metal dications. This observation is consistent with the proclivity of Zn^{2+} to bind to His residues in metalloproteins.

Acknowledgement. Financial support for this work was provided by the National Science Foundation, Grant CHE-2313553. The authors appreciatively acknowledge the *Nederlandse Organisatie voor Wetenschappelijk Onderzoek* (NWO) for the support of the FELIX Laboratory and a generous grant of computer time from the Center of High Performance Computing at the University of Utah. This manuscript is dedicated to Mary T. Rodgers in celebration of her collegiality and friendship and in thanks for introducing PBA to FELIX and IRMPD action spectroscopy.

References

Uncategorized References

- 1. Coleman, J. E., Zinc proteins: enzymes, storage proteins, transcription factors, and replication proteins. *Annual review of biochemistry* **1992**, 61, (1), 897-946.
- 2. Berg, J. M.; Shi, Y., The Galvanization of Biology: A Growing Appreciation for the Roles of Zinc. In *Science*, 1996; Vol. 271, pp 1081-1085.
- 3. Fairall, L.; Schwabe, J. W. R.; Chapman, L.; Finch, J. T.; Rhodes, D., The Crystal Structure of a Two Zinc-finger Peptide Reveals an Extension to the Rules for Zinc-finger/DNA Recognition. *Nature* **1993**, 366, 483 487.
- 4. Iuchi, S.; Kuldell, N., Zinc Finger Proteins From Atomic Contact to Cellular Function. Kluwer Academic/Plenum New York, 2005.
- 5. Li, X.; Han, M.; Zhang, H.; Liu, F.; Pan, Y.; Zhu, J.; Liao, Z.; Chen, X.; Zhang, B., Structures and biological functions of zinc finger proteins and their roles in hepatocellular carcinoma. *Biomarker Research* **2022**, 10, (1), 2.

- 6. Sigel, H.; Martin, R. B., Coordinating properties of the amide bond. Stability and structure of metal ion complexes of peptides and related ligands. *Chem. Rev.* **1982**, 82, (4), 385-426.
- 7. Dunbar, R. C.; Berden, G.; Oomens, J., How does a small peptide choose how to bind a metal ion? IRMPD and computational survey of CS versus Iminol binding preferences. *International Journal of Mass Spectrometry* **2013**, 354-355, 356-364.
- 8. Dunbar, R. C.; Martens, J.; Berden, G.; Oomens, J., Transition Metal(II) Complexes of Histidine-containing Tripeptides: Structures, and Infrared Spectroscopy by IRMPD. *Int. J Mass Spectrom.* **2018**, 429, 198-205.
- 9. Dunbar, R. C.; Steill, J. D.; Polfer, N. C.; Berden, G.; Oomens, J., Peptide Bond Tautomerization Induced by Divalent Metal Ions: Characterization of the Iminol Configuration. *Ang. Chem. Int. Ed.* **2012**, 51, (19), 4591-4593.
- 10. Malgieri, G.; Palmieri, M.; Esposito, S.; Maione, V.; Russo, L.; Baglivo, I.; de Paola, I.; Milardi, D.; Diana, D.; Zaccaro, L.; Pedone, P. V.; Fattorusso, R.; Isernia, C., Zinc to cadmium replacement in the prokaryotic zinc-finger domain. *Metallomics* **2014**, 6, (1), 96-104.
- 11. Malgieri, G.; Zaccaro, L.; Leone, M.; Bucci, E.; Esposito, S.; Baglivo, I.; Gatto, A. D.; Russo, L.; Scandurra, R.; Pedone, P. V.; Fattorusso, R.; Isernia, C., Zinc to cadmium replacement in the A. thaliana SUPERMAN Cys₂His₂ zinc finger induces structural rearrangements of typical DNA base determinant positions. *Biopolymers* **2011**, 95, (11), 801-810.
- 12. Hofstetter, T. E.; Howder, C.; Berden, G.; Oomens, J.; Armentrout, P. B., Structural Elucidation of Biological and Toxicological Complexes: Investigation of Monomeric and Dimeric Complexes of Histidine with Multiply Charged Transition Metal (Zn and Cd) Cations using IR Action Spectroscopy. *J. Phys. Chem. B* **2011**, 115, (43), 12648-12661.
- 13. Stevenson, B. C.; Martens, J.; Berden, G.; Oomens, J.; Schäfer, M.; Armentrout, P. B., IRMPD Spectroscopic and Theoretical Structural Investigations of Zinc and Cadmium Dications Bound to Histidine Dimers. *The Journal of Physical Chemistry A* **2020**, 124, (49), 10266-10276.
- 14. Stevenson, B. C.; Peckelsen, K.; Martens, J.; Berden, G.; Oomens, J.; Schäfer, M.; Armentrout, P. B., An investigation of inter-ligand coordination and flexibility: IRMPD spectroscopic and theoretical evaluation of calcium and nickel histidine dimers. *Journal of Molecular Spectroscopy* **2021**, 381, 111532.
- 15. Stevenson, B. C.; Berden, G.; Martens, J.; Oomens, J.; Armentrout, P. B., Determining gasphase chelation of zinc, cadmium, and copper cations with HisHis dipeptide using action spectroscopy and theoretical calculations. *International Journal of Mass Spectrometry* **2024**, 495, 117154.
- 16. Coates, R. A.; McNary. C. P.; Boles, G. C.; Berden, G.; Oomens, J.; Armentrout, P. B., Structural Characterization of Gas-Phase Cysteine and Cysteine Methyl Ester Complexes with Zinc and Cadmium Dications by Infrared Multiple Photon Dissociation Spectroscopy. *Phys. Chem. Chem. Phys.* **2015**, 17, 25799-25808.
- 17. Boles, G. C.; Stevenson, B. C.; Hightower, R. L.; Berden, G.; Oomens, J.; Armentrout, P. B., Zinc and cadmium complexation of L-methionine: An infrared multiple photon dissociation spectroscopy and theoretical study. *Journal of Mass Spectrometry* **2021**, 56, (4), e4580.
- 18. Boles, G. C.; Hightower, R. L.; Berden, G.; Oomens, J.; Armentrout, P. B., Zinc and Cadmium Complexation of 1-Threonine: An Infrared Multiple Photon Dissociation

- Spectroscopy and Theoretical Study. *The Journal of Physical Chemistry B* **2019**, 123, (44), 9343-9354.
- 19. Coates, R. A.; Boles, G. C.; McNary, C. P.; Berden, G.; Oomens, J.; Armentrout, P. B., Zn²⁺ and Cd²⁺ Cationized Serine Complexes: Infrared Multiple Photon Dissociation Spectroscopy and Density Functional Theory Investigations. *Phys. Chem. Chem. Phys.* **2016**, 18, 22434 22445.
- 20. Boles, G. C.; Hightower, R. L.; Coates, R. A.; McNary, C. P.; Berden, G.; Oomens, J.; Armentrout, P. B., Experimental and Theoretical Investigations of Infrared Multiple Photon Dissociation Spectra of Aspartic Acid Complexes with Zn²⁺ and Cd²⁺. *JPCB* **2018**, 122, 3836-3853.
- 21. Boles, G. C.; Owen, C. J.; Berden, G.; Oomens, J.; Armentrout, P. B., Experimental and Theoretical Investigations of Infrared Multiple Photon Dissociation Spectra of Glutamic Acid Complexes with Zn²⁺ and Cd²⁺. *Phys. Chem. Chem. Phys.* **2017**, 19, 12394 12406.
- 22. Boles, G. C.; Coates, R. A.; Berden, G.; Oomens, J.; Armentrout, P. B., Experimental and Theoretical Investigations of Infrared Multiple Photon Dissociation Spectra of Asparagine Complexes with Zn²⁺ and Cd²⁺ and Their Deamidation Processes. *JPCB* **2016**, 120, 12486-12500.
- 23. Boles, G. C. C., R. A.; Berden, G.; Oomens, J.; Armentrout, P. B., Experimental and Theoretical Investigations of Infrared Multiple Photon Dissociation Spectra of Glutamine Complexes with Zn²⁺ and Cd²⁺. *J. Phys. Chem. B* **2015**, 119, 11607–11617.
- 24. Owen, C. J.; Boles, G. C.; Berden, G.; Oomens, J.; Armentrout, P. B., Experimental and Theoretical Investigations of Infrared Multiple Photon Dissociation Spectra of Lysine Complexes with Zn²⁺ and Cd²⁺. *Eur. J. Mass Spectrom.* **2019**, 25, 97-111.
- 25. Chalifoux, A. M.; Boles, G. C.; Berden, G.; Oomens, J.; Armentrout, P. B., Experimental and Theoretical Investigations of Infrared Multiple Photon Dissociation Spectra of Arginine Complexes with Zn²⁺ and Cd²⁺. *PCCP* **2018**, 20, 20712-20725.
- 26. Stevenson, B. C.; Martens, J.; Berden, G.; Oomens, J.; Armentrout, P. B., Spectroscopic Investigation of the Metal Coordination of the Aromatic Amino Acids with Zinc and Cadmium. *J. Phys. Chem. A* **2023**, 127, 3560-3569.
- 27. Dunbar, R. C.; Steill, J. D.; Polfer, N. C.; Oomens, J., Dimeric Complexes of Tryptophan with M²⁺ Metal Ions. *The Journal of Physical Chemistry A* **2009**, 113, (5), 845-851.
- 28. Oepts, D.; van der Meer, A. F. G.; van Amersfoort, P. W., The Free-Electron-Laser User Facility FELIX. *Infrared Phys. Technol.* **1995,** 36, 297-308.
- 29. Martens, J.; Berden, G.; Gebhardt, C. R.; Oomens, J., Infrared ion spectroscopy in a modified quadrupole ion trap mass spectrometer at the FELIX free electron laser laboratory. *Review of Scientific Instruments* **2016**, 87, (10), 103108.
- 30. Valle, J. J.; Eyler, J. R.; Oomens, J.; Moore, D. T.; van der Meer, A. F. G.; von Heldon, G.; Meijer, G.; Hendrickson, C. L.; Marshall, A. G.; Blakney, G. T., Free Electron Laser-Fourier Transform Ion Cyclotron Resonance Mass Spectrometry Facility for Obtaining Infrared Multiphoton Dissociation Spectra of Gaseous Ions. *Rev. Sci. Instrum.* 2005, 76, 023103.
- 31. Polfer, N. C. J. O., Reaction products in mass spectrometry elucidated with infrared spectroscopy. *Phys. Chem. Chem. Phys.* **2007**, 9, 3804-3817.
- 32. Berden, G.; Derksen, M.; Houthuijs, K. J.; Martens, J.; Oomens, J., An Automatic Variable Laser Attenuator for IRMPD Spectroscopy and Analysis of Power-dependence in Fragmentation Spectra. *International Journal of Mass Spectrometry* **2019**, 443, 1-8.

- 33. Lemaire, J.; Boissel, P.; Heninger, M.; Mauclaire, G.; Bellec, G.; Mestdagh, H.; Le Caer, S.; Ortega, J.; Glotin, F.; Maître, P., Gas Phase Infrared Spectroscopy of Selectively Prepared Ions. *Phys. Rev. Lett.* **2002**, 89, 273002.
- 34. Moision, R. M.; Armentrout, P. B., The Special Five-membered Ring of Proline: An Experimental and Theoretical Investigation of Alkali Metal Cation Interactions with Proline and Its Four- and Six-membered Ring Analogues. *J. Phys. Chem. A* **2006**, 110, 3933-3946.
- 35. McNary, C. P.; Armentrout, P. B., Threshold Collision-Induced Dissociation of Proton-Bound Hydrazine and Dimethylhydrazine Clusters. *JPCA* **2016**, 120, 9690-9701.
- 36. McNary, C. P.; Nei, Y.-w.; Maitre, P.; Rodgers, M. T.; Armentrout, P. B., Infrared Multiple Photon Dissociation Spectroscopy of Protonated Glycine, Lysine, Histidine, and Arginine Complexed with 18-Crown-6. *PCCP* **2019**, 21, 12625-12639.
- 37. Valiev, M.; Bylaska, E. J.; Govind, N.; Kowalski, K.; Straatsma, T. P.; Van Dam, H. J. J.; Wang, D.; Nieplocha, J.; Apra, E.; al., E., NWChem: A comprehensive and scalable open-source solution for large scale molecular simulations. *Computer Physics Communications* **2010**, 181, 1477-1489.
- 38. Case, D. A.; Babin, V.; Berryman, J. T.; Betz, R. M.; Cai, Q.; Cerutti, D. S.; Cheatham, T. E.; Darden, T. A.; Duke, R. E.; Gohlke, H.; Goetz, A. W.; Gusarov, S.; Homeyer, N.; Janowski, P.; Kaus, J.; Kolossváry, I.; Kovalenko, A.; Lee, T. S.; LeGrand, S.; Luchko, T.; Luo, R.; Madej, B.; Merz, K. M.; Paesani, F.; Roe, D. R.; Roitberg, A.; Sagui, C.; Salomon-Ferrer, R.; Seabra, G.; Simmerling, C. L.; Smith, W.; Swails, J.; Walker, R. C.; Wang, J.; Wolf, R. M.; Wu, X.; Kollman, P. A. *AMBER 14*, University of California: San Francisco, 2014.
- 39. Frisch, M. J.; Trucks, G. W.; Schlegel, H. B.; Scuseria, G. E.; Robb, M. A.; Cheeseman, J. R.; Scalmani, G.; Barone, V.; Petersson, G. A.; Nakatsuji, H.; Li, X.; Caricato, M.; Marenich, A. V.; Bloino, J.; Janesko, B. G.; Gomperts, R.; Mennucci, B.; Hratchian, H. P.; Ortiz, J. V.; Izmaylov, A. F.; Sonnenberg, J. L.; Williams-Young, D.; Ding, F.; Lipparini, F.; Egidi, F.; Goings, J.; Peng, B.; Petrone, A.; Henderson, T.; Ranasinghe, D.; Zakrzewski, V. G.; Gao, J.; Rega, N.; Zheng, G.; Liang, W.; Hada, M.; Ehara, M.; Toyota, K.; Fukuda, R.; Hasegawa, J.; Ishida, M.; Nakajima, T.; Honda, Y.; Kitao, O.; Nakai, H.; Vreven, T.; Throssell, K.; J. A. Montgomery, J.; Peralta, J. E.; Ogliaro, F.; Bearpark, M. J.; Heyd, J. J.; Brothers, E. N.; Kudin, K. N.; Staroverov, V. N.; Keith, T. A.; Kobayashi, R.; Normand, J.; Raghavachari, K.; Rendell, A. P.; Burant, J. C.; Iyengar, S. S.; Tomasi, J.; Cossi, M.; Millam, J. M.; Klene, M.; Adamo, C.; Cammi, R.; Ochterski, J. W.; Martin, R. L.; Morokuma, K.; Farkas, O.; Foresman, J. B.; Fox, D. J. *Gaussian 16, Revision A.03*, Gaussian, Inc.: Wallingford CT, 2016.
- 40. Becke, A. D., Density-functional Thermochemistry. III. The Role of Exact Exchange. *J. Chem. Phys.* **1993**, 98, 5648-5652.
- 41. Lee, C.; Yang, W.; Parr, R. G., Development of the Colle-Salvetti Correlation-Energy Formula into a Functional of the Electron Density. *Phys. Rev. B* **1988**, 37, 785-789.
- 42. Weigend, F.; Ahlrichs, R., Balanced basis sets of split valence, triple zeta valence and quadruple zeta valence quality for H to Rn: Design and assessment of accuracy. *Phys. Chem. Chem. Phys.* **2005**, 7, (18), 3297-3305.
- 43. Andrae, D.; Haeussermann, U.; Dolg, M.; Stoll, H.; Preuss, H., Energy-adjusted Ab Initio Pseudopotentials for the Second and Third Row Transition Elements. *Theor. Chim. Acta* **1990,** 77, 123-141.

- 44. Pritchard, B. P.; Altarawy, D.; Didier, B.; Gibson, T. D.; Windus, T. L., A New Basis Set Exchange: An Open, Up-to-date Resource for the Molecular Sciences Community. *J. Chem. Inf. Model.* **2019**, 59, (11), 4814-4820.
- 45. Polfer, N. C., Infrared Multiple Photon Dissociation Spectroscopy of Trapped Ions. *Chem. Soc. Rev.* **2011,** 40, 2211–2221.
- 46. Kesharwani, M. K.; Brauer, B.; Martin, J. M. L., Frequency and Zero-Point Vibrational Energy Scale Factors for Double-Hybrid Density Functionals (and Other Selected Methods): Can Anharmonic Force Fields Be Avoided? *J. Phys. Chem. A* **2015**, 119, (9), 1701-1714.
- 47. Grimme, S. E., S.; Goerigk, L., Effect of the Damping Function in Dispersion Corrected Density Functional Theory. *J. Comput. Chem.* **2011**, 32, (7), 1456-1465.
- 48. Grimme, S. A., J.; Ehrlich, S.; Krieg, H., A Consistent and Accurate Ab Initio Parametrization of Density Functional Dispersion Correction (DFT-D) for the 94 Elements H-Pu. *J. Chem. Phys.* **2010**, 132, (15), 154104-154119.
- 49. Armentrout, P. B.; Rodgers, M. T.; Oomens, J.; Steill, J. D., Infrared Multiphoton Dissociation Spectroscopy of Cationized Serine: Effects of Alkali-Metal Cation Size on Gas-Phase Conformation. *J. Phys. Chem. A* **2008**, 112, 2248-2257.
- 50. Rodgers, M. T.; Armentrout, P. B.; Oomens, J.; Steill, J. D., Infrared Multiphoton Dissociation Spectroscopy of Cationized Threonine: Effects of Alkali-Metal Cation Size on Gas-Phase Conformation. *J. Phys. Chem. A* **2008**, 112, 2258-2267.
- 51. Citir, M. H., C. S.; Oomens, J.; Steill, J. D.; Armentrout, P. B., Infrared Multiple Photon Dissociation Spectroscopy of Cationized Histidine: Effects of Metal Cation Size on Gas-Phase Conformation. *J. Phys. Chem. A* **2012**, 116, 1532-1541.
- 52. Citir, M.; Stennett, E. M. S.; Oomens, J.; Steill, J. D.; Rodgers, M. T.; Armentrout, P. B., Infrared Multiple Photon Dissociation Spectroscopy of Cationized Cysteine: Effects of Metal Cation Size on Gas-Phase Conformation. *Int. J. Mass Spectrom.* **2010**, 297, 9-17.
- 53. Rodrigues-Oliveira, A. F.; M. Ribeiro, F. W.; Cervi, G.; C. Correra, T., Evaluation of Common Theoretical Methods for Predicting Infrared Multiphotonic Dissociation Vibrational Spectra of Intramolecular Hydrogen-Bonded Ions. *ACS Omega* **2018**, 3, (8), 9075-9085.
- 54. Dunbar, R. C.; Oomens, J.; Berden, G.; Lau, J. K.-C.; Verkerk, U. H.; Hopkinson, A. C.; Siu, K. W. M., Metal Ion Complexes with HisGly: Comparison with PhePhe and PheGly. *The Journal of Physical Chemistry A* **2013**, 117, (25), 5335-5343.

Table 1. Relative Enthalpies at 0 K (Gibbs Energies at 298 K) of Zn²⁺(AAH) in kJ/mol

Cturrotrum	D21 VD	B3LYP-	B3P86	MD2(6,11)	
Structure	B3LYP	GD3BJ	D3P80	MP2(full)	
$[N_\alpha,N^2,N^3,CO^3,N_\pi]\text{-ct}_ctct_cttt$	0.2 (0.0)	0.0 (0.0)	0.0 (0.0)	0.0 (0.0)	
$[N_\alpha,CO^1,CO^2,N_\pi]\text{-gtcttttt}$	0.0 (1.2)	3.5 (5.2)	5.8 (7.1)	18.2 (19.6)	
$[N_\alpha, CO^1, CO^3, N_\pi]\text{-ttggtctt}$	12.0 (14.3)	4.4 (7.9)	16.5 (19.0)	21.8 (24.3)	

Table 2. Relative Enthalpies at 0 K (Gibbs Energies at 298 K) of Cd²⁺(AAH) in kJ/mol

Structure	B3LYP	_		MP2(full)
		GD3BJ		
$[N_\alpha,CO^1,CO^2,N_\pi]\text{-gtcttttt}$	0.0 (0.0)	0.0 (0.0)	0.0 (0.0)	1.0 (2.5)
$[N_\alpha,N^2,N^3,CO^3,N_\pi]\text{-}ct_ctct_cttt$	14.6 (13.2)	12.2 (10.4)	9.3 (7.8)	0.0 (0.0)
$[N_\alpha, CO^1, CO^3, N_\pi]\text{-}gtggtgtt$	23.7 (23.8)	13.8 (14.3)	22.9 (23.1)	19.4 (20.9)

Table 3. Relative Enthalpies at 0 K (Gibbs Energies at 298 K) of Zn²⁺(AHA) in kJ/mol

Ch	D2LVD	B3LYP-	D2D07	MD2(C 11)	
Structure	B3LYP	GD3BJ	B3P86	MP2(full)	
$[N_\alpha, N^2, N^3, CO^3]\text{-ctcttttt}$	0.0(0.0)	12.6 (10.0)	1.2 (0.0)	30.4 (25.0)	
$[N_\alpha, N^2, N^3, CO^3]\text{-cttct}_cttt$	1.2 (4.6)	13.2 (10.6)	1.8 (4.0)	32.1 (30.2)	
$[N_\alpha, N^2, N_\pi, N^3, CO^3]\text{-}ct_cgct_cttt$	2.6 (8.0)	0.0 (0.0)	0.0 (4.1)	0.0 (0.0)	
$[CO^1, N_\pi, N^3H, CO^3]\text{-ctcgtgtt}$	19.5 (25.3)	19.6 (19.5)	21.2 (25.8)	33.7 (34.2)	
$[N_{\alpha}, CO^1, CO^2, CO^3]$ -gtgttggt	54.7 (62.8)	55.0 (58.0)	52.2 (59.1)	69.8 (72.6)	

Table 4. Relative Enthalpies at 0 K (Gibbs Energies at 298 K) of Cd²⁺(AHA) in kJ/mol

Structure	B3LYP	B3LYP-	B3P86	MP2(full)	
		GD3BJ			
$[N_{\alpha}, N^2, N^3, CO^3]$ -ctcttttt	0.0(0.0)	3.2 (4.1)	0.0(0.0)	20.5 (23.2)	
$[N_{\alpha}, N^2, N^3, CO^3]$ -cttctcttt	1.1 (0.1)	5.4 (5.3)	1.6 (0.4)	21.6 (23.1)	
$[N_\alpha,N^2,N_\pi,N^3,CO^3]\text{-}ct_ctct_tttt$	10.8 (11.7)	0.0 (2.0)	9.9 (10.8)	0.0 (3.6)	
$[N_\alpha,N^2,N_\pi,N^3,CO^3]\text{-}ct_cgct_cttt$	8.5 (5.0)	0.3 (0.0)	7.7 (4.2)	0.9 (0.0)	
$[CO^1,N_\pi,N^3H,CO^3]\text{-ctcgtgtt}$	24.2 (23.8)	16.3 (17.6)	26.9 (26.4)	29.0 (31.2)	
$[N_\alpha,CO^1,CO^2,CO^3]\text{-}gtgttggt$	37.0 (38.7)	33.2 (37.5)	39.3 (40.9)	50.6 (54.9)	

Table 5. Relative Enthalpies at 0 K (Gibbs Energies at 298 K) of Zn²⁺(HAA) in kJ/mol

Structure	B3LYP	B3LYP- GD3BJ	B3P86	MP2(full)
$[N_\alpha,N_\pi,N^2,N^3,CO^3]\text{-}ct_ctct_cttt$	0.0 (0.0)	0.0 (0.0)	0.0 (0.0)	0.0 (0.0)
$[N_\alpha, N_\pi, CO^1, CO^3]\text{-gtcttgtt}$	3.5 (3.2)	0.7 (1.4)	7.8 (7.5)	13.1 (12.8)
$[N_\alpha, N_\pi, CO^1, CO^3]\text{-}gtggtggc$	25.3 (29.7)	17.8 (23.5)	28.1 (32.5)	32.5 (36.9)
$[N_\alpha, N_\pi, CO^1, CO^2, CO^3]\text{-ttcttgtt}$	30.3 (30.3)	21.9 (23.8)	31.1 (31.1)	33.2 (33.2)

Table 6. Relative Enthalpies at 0 K (Gibbs Energies at 298 K) of Cd²⁺(HAA) in kJ/mol

Structure	B3LYP	B3LYP- GD3BJ	B3P86	MP2(full)
$[N_{\alpha}, N_{\pi}, CO^{1}, CO^{2}, CO^{3}]$ -gtettggt	0.0 (0.0)	0.0 (0.0)	0.0 (0.0)	0.0(0.0)
$[N_\alpha,N_\pi,N^2,N^3,CO^3]\text{-}ct_ctct_cttt$	12.9 (10.4)	16.7 (14.0)	11.2 (8.7)	6.6 (4.1)
$[N_\alpha, N_\pi, CO^1, CO^3]\text{-}gtggtggc$	24.8 (27.6)	20.9 (24.2)	24.8 (27.6)	24.0 (26.9)

Table 7. Assignments for each complex with comparison to the previous study of Dunbar et al.[8] IM represents iminol. CS represents charge-solvated.

	Ni ²⁺	Cu^{2+}	Zn^{2+}	Cd^{2+}
AAH	IM + CS	IM	IM + CS	CS + IM
AHA	IM	IM	IM	IM
HAA	IM	$CS (+IM)^a$	CS	CS

^a Parentheses indicate that the CS conformer was confidently assigned, but spectral overlap did not allow the IM to be eliminated.

Figure Captions

Figure 1. Structures of Zn²⁺(AAH) conformers calculated at B3LYP/6-311+G(d,p) level of theory. Dashed grey lines indicate hydrogen bonds and yellow dashed lines indicate metal-ligand interactions. (Gray, carbon; white, hydrogen; red, oxygen; blue, nitrogen; steel gray, zinc).

Figure 2. Structures of Zn²⁺(AHA) conformers calculated at B3LYP/6-311+G(d,p) level of theory and one unique Cd²⁺(AHA) complex calculated at the B3LYP/def2-TZVP level. Dashed grey lines indicate hydrogen bonds and yellow dashed lines indicate metal-ligand interactions. (Gray, carbon; white, hydrogen; red, oxygen; blue, nitrogen; steel gray, zinc; yellow, cadmium).

Figure 3. Structures of Zn²⁺(HAA) conformers calculated at B3LYP/6-311+G(d,p) level of theory and one unique Cd²⁺(HAA) complex calculated at the B3LYP/def2-TZVP level. Dashed grey lines indicate hydrogen bonds and yellow dashed lines indicate metal-ligand interactions. (Gray, carbon; white, hydrogen; red, oxygen; blue, nitrogen; steel gray, zinc; yellow, cadmium).

Figure 4. Comparison of the Zn²⁺(AAH) experimental IRMPD spectrum from QIT (black and gray dashed lines) and Zn²⁺(AAH) experimental IRMPD spectrum from FTICR (red and red dashed lines) with calculated spectra at the B3LYP/6-311+G(d,p) level of theory for low-lying conformers. Relative 298 K Gibbs energies (kJ/mol) are given at the B3LYP, B3LYP-GD3BJ, B3P86, and MP2 levels, respectively, using the 6-311+G(2d,2p) basis set.

Figure 5. Comparison of the Cd²⁺(AAH) experimental IRMPD spectrum (black and gray dashed lines), Zn²⁺(AAH) experimental (dark purple), and calculated spectra at the B3LYP/def2-TZVP level of theory for low-lying conformers. Relative 298 K Gibbs energies (kJ/mol) are given at the B3LYP, B3LYP-GD3BJ, B3P86, and MP2 levels, respectively, using the def2-TZVPP basis set.

Figure 6. Comparison of the Zn²⁺(AHA) experimental IRMPD spectrum (black and gray dashed lines) with calculated spectra at the B3LYP/6-311+G(d,p) level of theory for low-lying conformers. Relative 298 K Gibbs energies (kJ/mol) are given at the B3LYP, B3LYP-GD3BJ, B3P86, and MP2 levels, respectively, using the 6-311+G(2d,2p) basis set.

Figure 7. Comparison of the Cd²⁺(AHA) experimental IRMPD spectrum (black and gray dashed lines), Zn²⁺(AHA) experimental (dark purple), and calculated spectra at the B3LYP/def2-TZVP level of theory for low-lying conformers. Relative 298 K Gibbs energies (kJ/mol) are given at the B3LYP, B3LYP-GD3BJ, B3P86, and MP2 levels, respectively, using the def2-TZVPP basis set.

Figure 8. Comparison of the Zn²⁺(HAA) experimental IRMPD spectrum (black, red scaled up by 10 at low wavenumber, and gray dashed lines) with calculated spectra at the B3LYP/6-311+G(d,p) level of theory for low-lying conformers. Relative 298 K Gibbs energies (kJ/mol) are given at the B3LYP, B3LYP-GD3BJ, B3P86, and MP2 levels, respectively, using the 6-311+G(2d,2p) basis set.

Figure 9. Comparison of the Cd²⁺(HAA) experimental IRMPD spectrum (black, red scaled up by 10 at low wavenumber, and gray dashed lines), Zn²⁺(HAA) experimental (dark purple), and calculated spectra at the B3LYP/def2-TZVP level of theory for low-lying conformers. Relative 298 K Gibbs energies (kJ/mol) are given at the B3LYP, B3LYP-GD3BJ, B3P86, and MP2 levels, respectively, using the def2-TZVPP basis set.

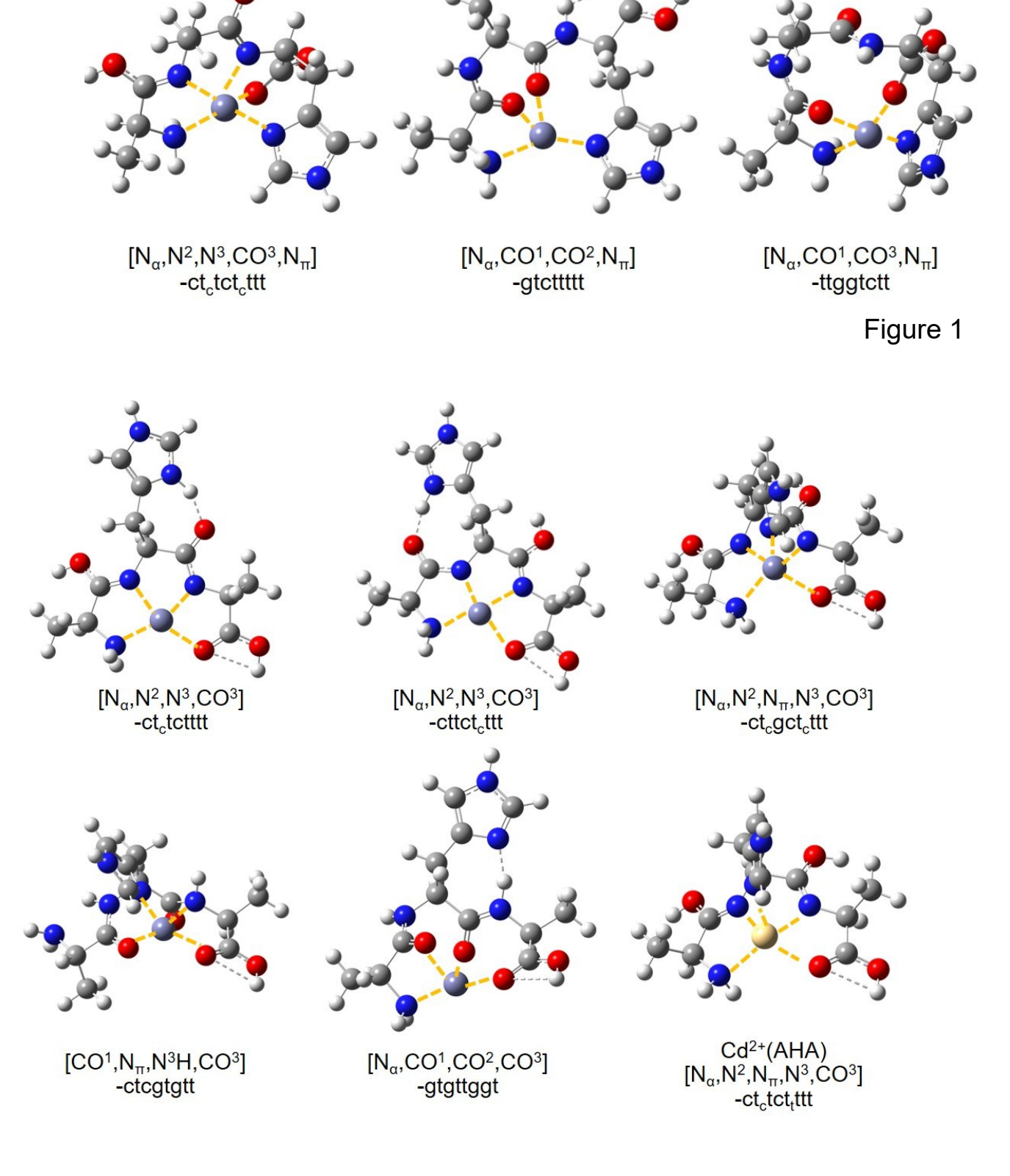


Figure 2

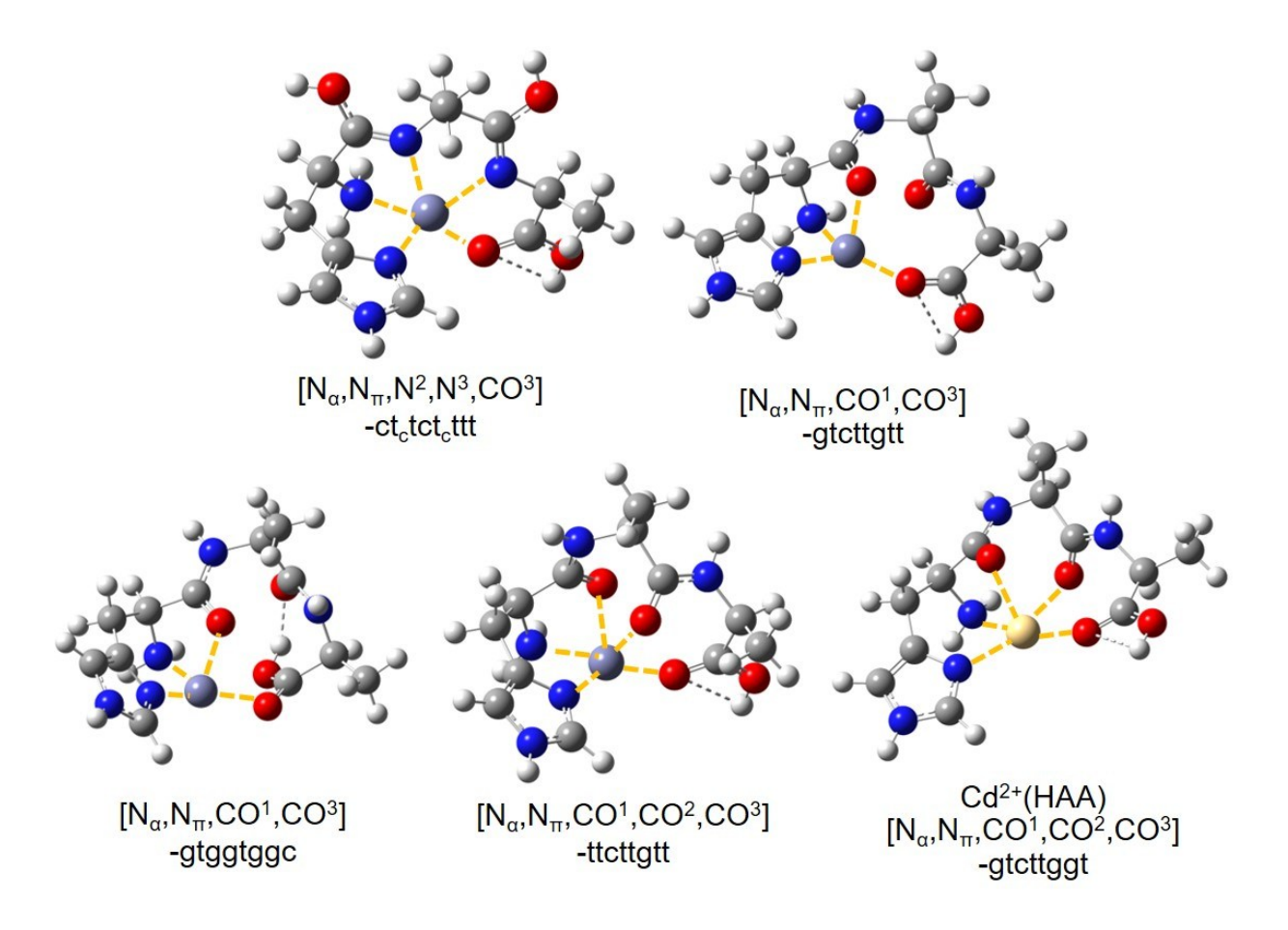
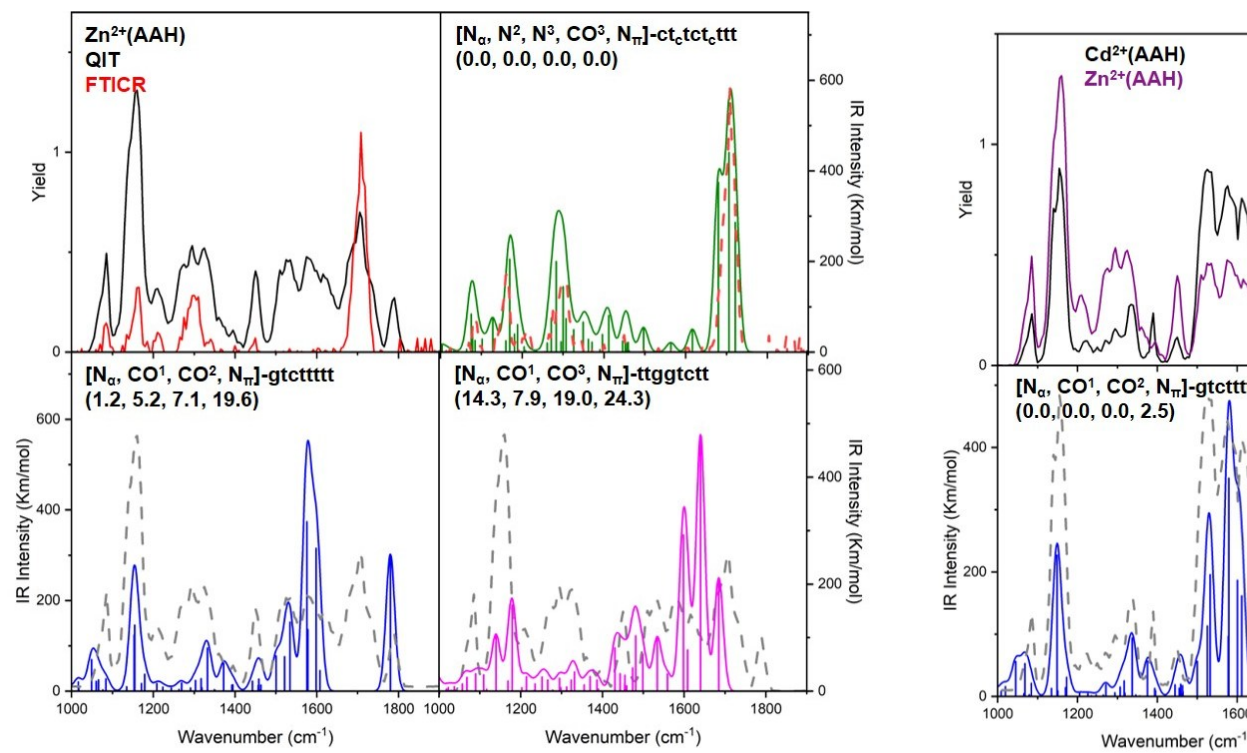


Figure 3



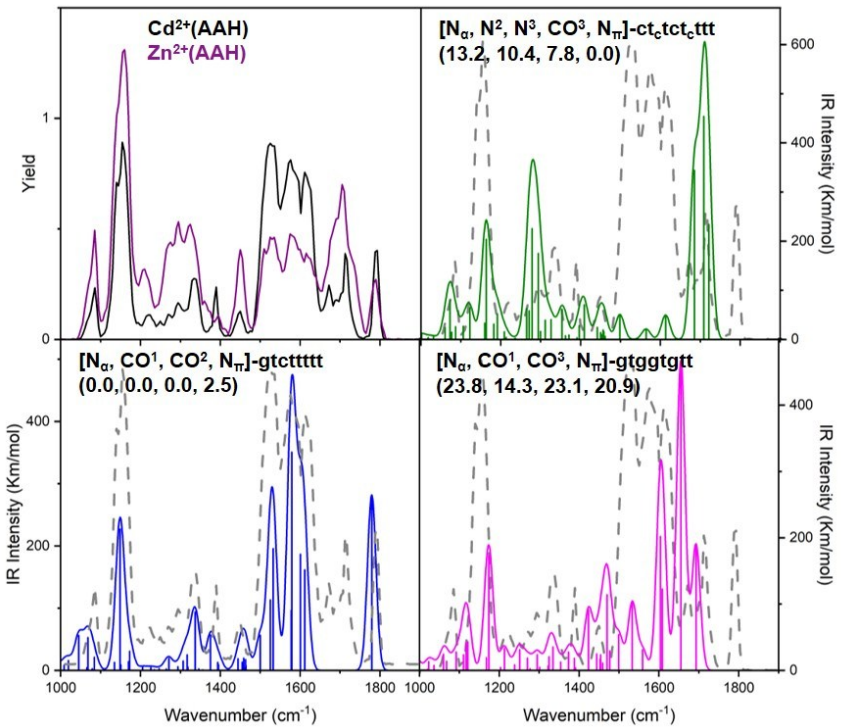
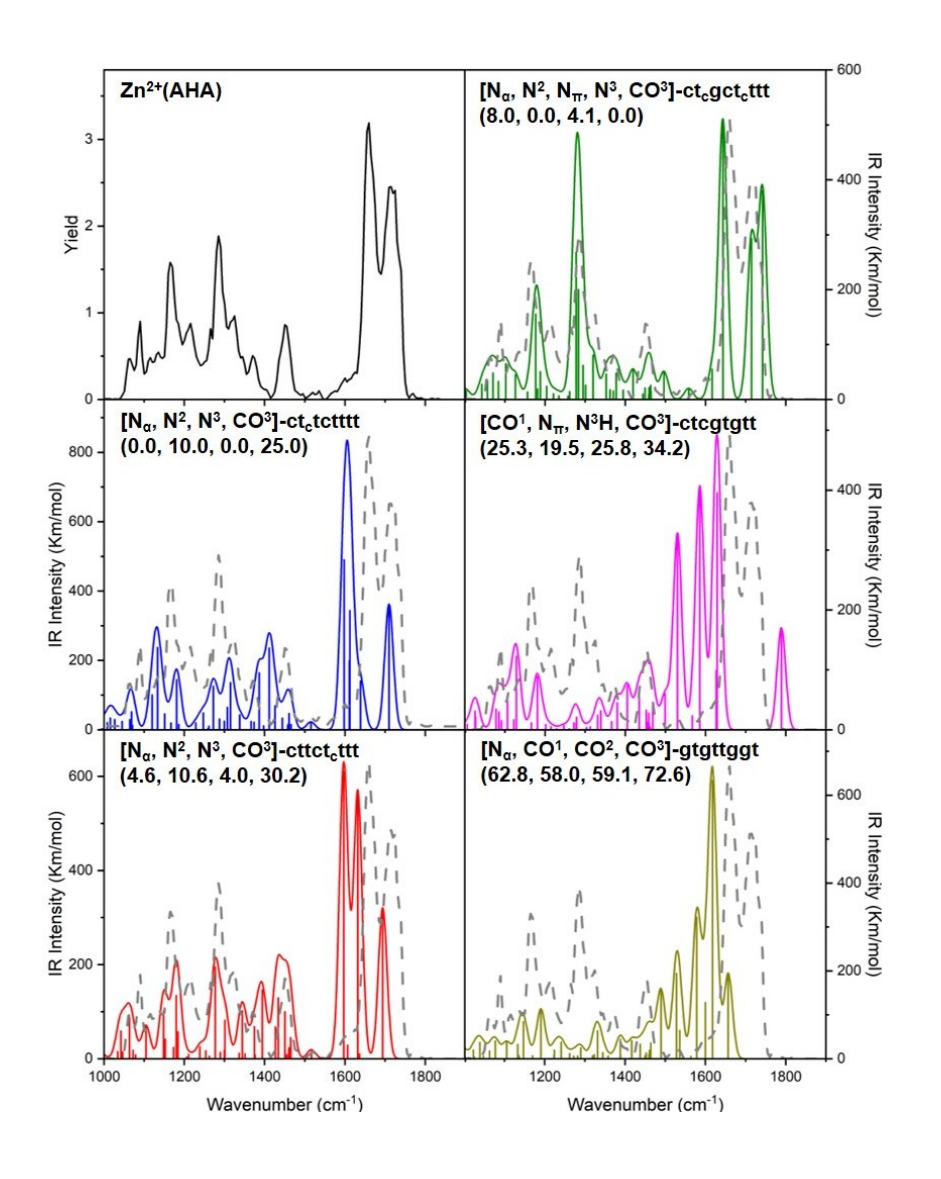


Figure 4 Figure 5



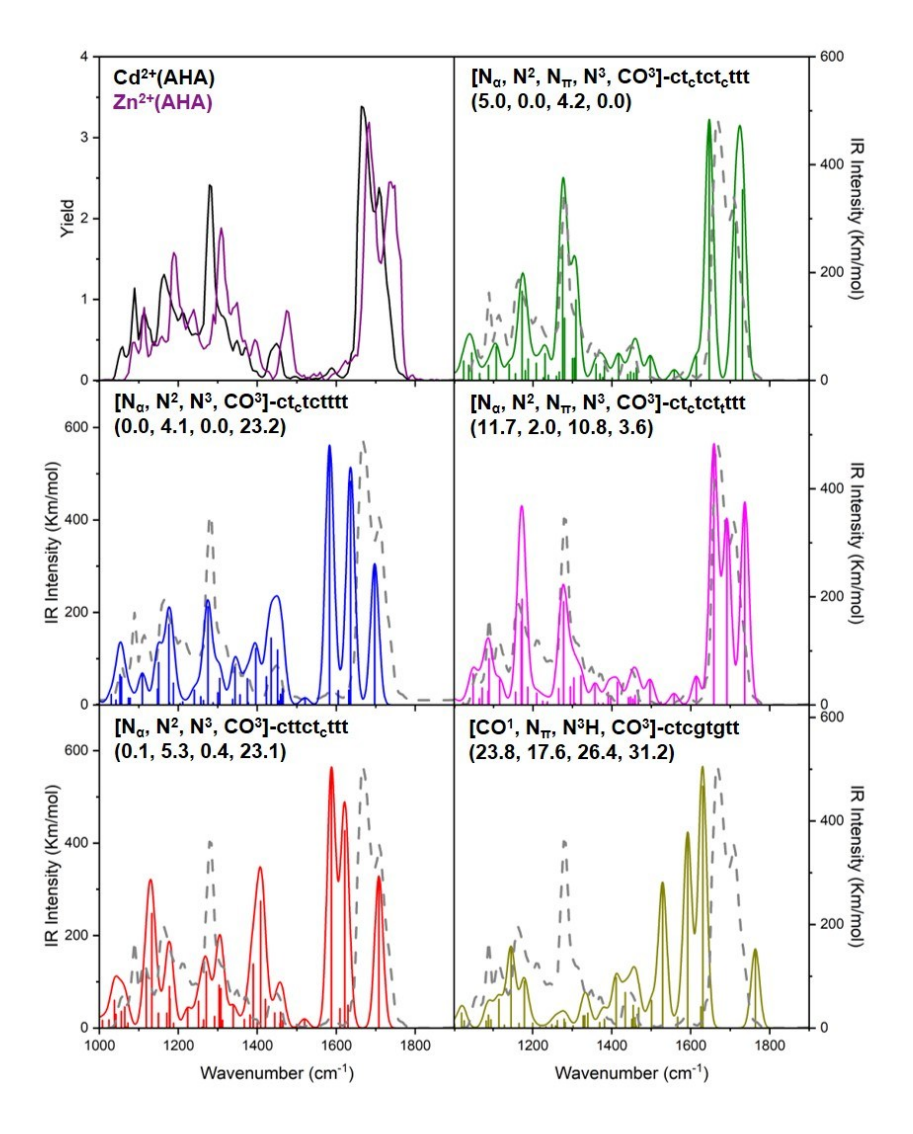


Figure 6 Figure 7

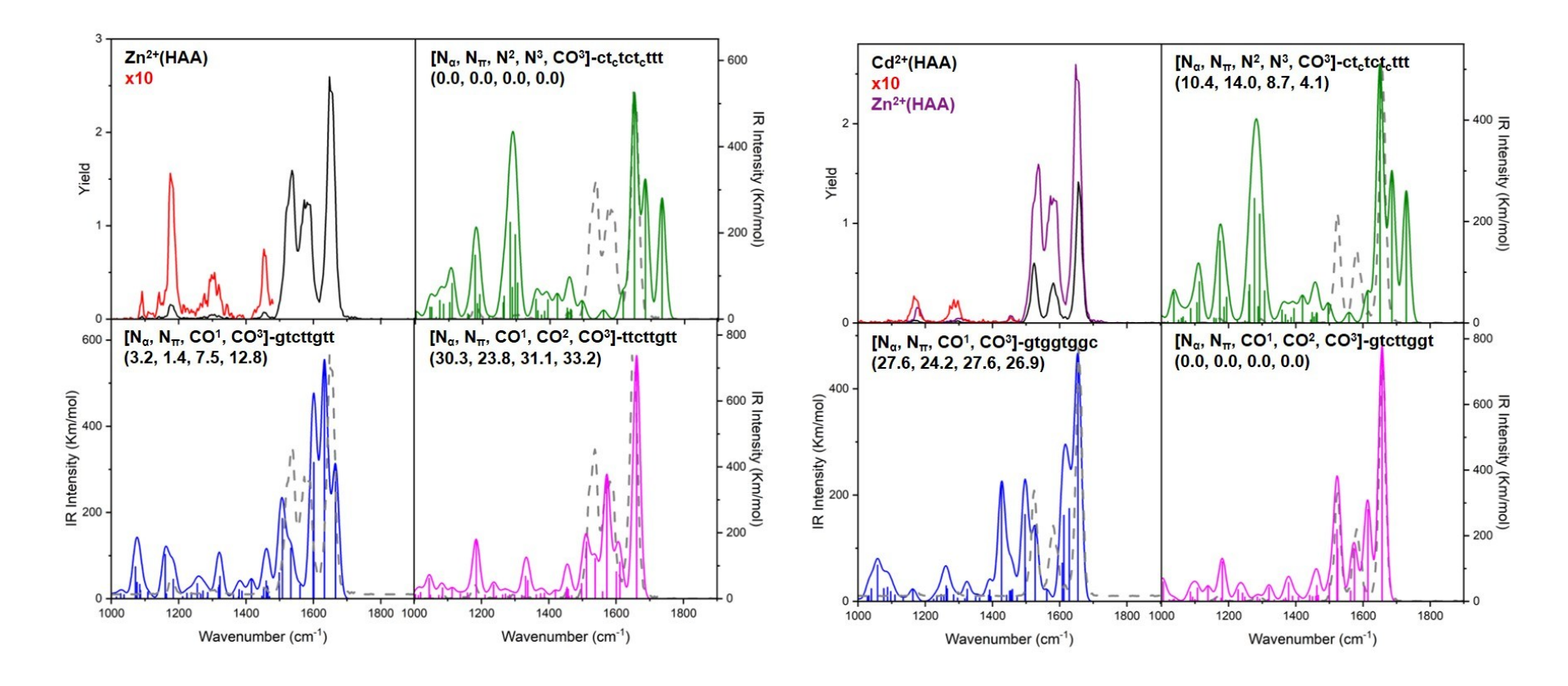


Figure 8 Figure 9